Wind and Structures, Vol. 1, No. 3 (1998) 271-284
DOI: http://dx.doi.org/10.12989/was.1998.1.3.271

Three-dimensional numerical simulation of turbulent flow around two high-rise buildings in proximity

Min-Shan Liu†

Department of Mechanical Engineering, Feng-Chia University
Taichung, 40725, Taiwan, R.O.C.

Abstract. This paper uses the numerical simulation to investigate the interference effect of 3-D turbulent flow around two high rise buildings in proximity at the different relative heights, gaps, and wind velocities. The computer program used to carry out the simulation is based on the control volume method and the SIMPLEST algorithm. The k-ε model was used to simulate turbulence effects. Since the contracted flow between two adjacent buildings enhances the strength of vortex shedding from the object building, the pressure coefficient on each side wall of the object building is generally increased by the presence of apposed building. The effect is increased as the relative height or the gap between the two buildings decreases. The velocity on the vertical center line between two buildings is about 1.4 to 1.5 times the upstream wind velocity.

Key words: high rise buildings; SIMPLEST; k-ε model.

1. Introduction

Due to the limited land resources, many high rise buildings are constructed in a high density in the megalopolis area throughout the world. Neighboring buildings may exhibit significant interaction effects on the buildings and surrounding.

For examples :

1) The wind induced shear stress and the pressure force are the important causes of the damage of building structures, the glass windows or the cladding elements on the outside wall, and the loft garden on the top of the building.
2) High rise buildings would induce and strengthen the wind velocity on the ground, to create the inconveniences of the pedestrians and even a dangerous circumstance.
3) The stresses of wind would bring about the vibration of the high rise building, making the building occupants feel uncomfort.
4) At the factory nearby or the high density construction area, the diffusion of polluted air or discarded air is strongly related to the arrangement of buildings.
5) The pressure distribution around the building would influence the ventilation of each room of the building.

Therefore, the study on interference effects of the wind on the two closely located high rise

† Assistant Professor

buildings are one of the important problems. Traditionally, these wind related data were collected in wind tunnels using scale models such as the work by Taniike (1992). Today, due to the improvement in computer performance and the progress in computational fiuid dynamics (CFD), more scientists use the numerical simulation to investigate into the wind flow field such as the works by Murakami and Mochida (1989), Stathopoulos and Zhou (1993), Qasim, Maxwell and Parameswaran (1992) for a single building, Patersons and Apelt (1989) for two neighboring buildings.

2. The physical mode and the numerical method

The physical model is shown in Fig. 1. Both the interfering building B1 and the object building B2 are the exactly square pillar of the breadth of 30 m. B2 is 150 m high which equals to five times the breadth of the buildings. In the test, B1 had three different heights, i.e., 75, 100, and 150 m. The gaps between two buildings are 15, 30, and 45 m. The upstream wind velocities U were 10, 15, and 20 m/s corresponding to scale 5, 7, and 8 wind. Buildings are oriented with one face of each building normal to the wind.

If we denote the width of the building with w, then the distance of wind entrance to the front surface of the building L1 was 3w. The distance L2, from the building's back surface to the limit of computational domain equals to 10w. The distances between the side surfaces of building and computational boundary L4 and L5 were 3w. The distance between the roof and computational boundary L3 was 5w. The simulation was carried out with and without interfering building.

This paper uses the two-equation k-ε turbulence model from Launder and Spalding (1974). The governing equations are the time-averaged continuity, momentum (Navier-Stokes) and the k - ε model turbulence equations.

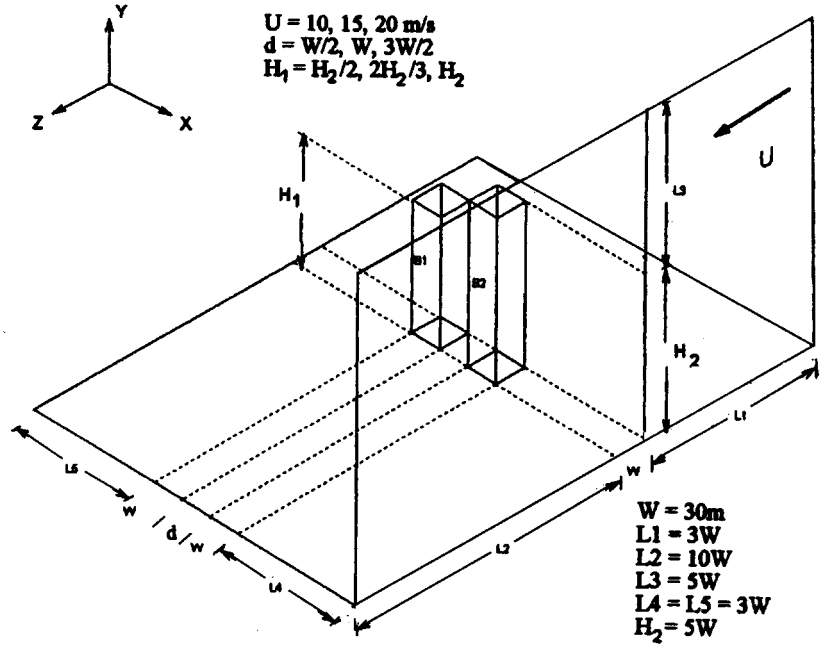

Fig. 1 The physical model

Continuity Equation ;

$$\frac{\partial \overline{u_i}}{\partial x_i} = 0 \tag{1}$$

Navier-Stokes Equations ;

$$\frac{\partial \overline{u_i}\,\overline{u_j}}{\partial x_j} = -\frac{\partial}{\partial x_j}\left(\frac{\overline{P}}{\rho} + \frac{2}{3}\kappa\right) + \frac{\partial}{\partial x_i}\left[\nu_i\left(\frac{\partial \overline{u_i}}{\partial x_j} + \frac{\partial \overline{u_j}}{\partial x_i}\right)\right] \tag{2}$$

Transport equation for the turbulent kinetic energy ;

$$\frac{\partial \kappa \overline{u_j}}{\partial x_j} = \frac{\partial}{\partial x_j}\left(\frac{\nu_t}{\sigma_\kappa}\frac{\partial \kappa}{\partial x_j}\right) + \nu_t S - \varepsilon \tag{3}$$

Transport equation for the dissipation rate of turbulent kinetic energy ;

$$\frac{\partial \varepsilon \overline{u_j}}{\partial x_j} = \frac{\partial}{\partial x_j}\left(\frac{\nu_t}{\sigma_\varepsilon}\frac{\partial \varepsilon}{\partial x_j}\right) + C_1\frac{\varepsilon}{\kappa}\nu_t S - C_2\frac{\varepsilon^2}{\kappa} \tag{4}$$

where :

$$S = \left(\frac{\partial \overline{u_i}}{\partial x_j} + \frac{\partial \overline{u_j}}{\partial x_i}\right)\frac{\partial \overline{u_i}}{\partial x_j} \tag{5}$$

$$\nu_t = C_\mu\frac{\kappa^2}{\varepsilon} = \text{turbulent kinematic viscosity} \tag{6}$$

$$\kappa = \frac{1}{2}\overline{u_i' u_j'} = \text{turbulent kinetic energy} = \frac{3}{2}I^2U^2 \tag{7}$$

$$\varepsilon = \nu\overline{\left(\frac{\partial u_i'}{\partial x_j}\right)^2} = \text{dissipation rate} = \frac{C_\mu \kappa^2}{\nu_t} \tag{8}$$

and I is the turbulence intensity, U is the upstream wind velocity, κ is the turbulence energy, and ε is the dissipation rate of the turbulence energy. The turbulence model constants are provided in Table 1 (Launder and Spalding 1974). The turbulence intensity I of upstream wind at the inlet boundary is 0.06.

On the building surfaces and the ground, the wall function method described by Launder and Spalding (1974) is used to prescribe the boundary conditions for the velocity and turbulence quantities, assuming that the turbulence is in the state of local equilibrium. At the outlet boundaries,

Table 1 Turbulence model constants

C_μ	σ_κ	σ_ε	C_1	C_2
0.09	1.0	1.3	1.44	1.92

all the quantity gradients are zeros except the velocity component of Z direction, At the inlet boundary, a uniform profile of all the dependent variables are specified.

These governing equations associated with the boundary conditions were solved numerically by the control volume finite difference method. The governing equations were transformed into the discrete from, i.e., an algebraic form. By integrating over the space for each control volume, the result is of the following general form :

$$a_p \phi_p = \sum_{nb} a_{nb} \phi_{nb} + b$$

where a_p and a_{nb} are discrete transport coefficients, ϕ is a general dependent variable, b is the source term and subscripts p and nb refer to a specific control volume and neighboring control volumes, respectively. The adopted solution method for the velocity-pressure fields is the SIMPLEST algorithm proposed by Patankar (1981).

A grid independent solution for the cases in this study was obtained by using $35 \times 35 \times 41$ non-uniform staggered Cartesian grid system in the computational domain as shown in Fig. 2. The finest grid was used near the wall surface to ensure that the first node near the wall be in

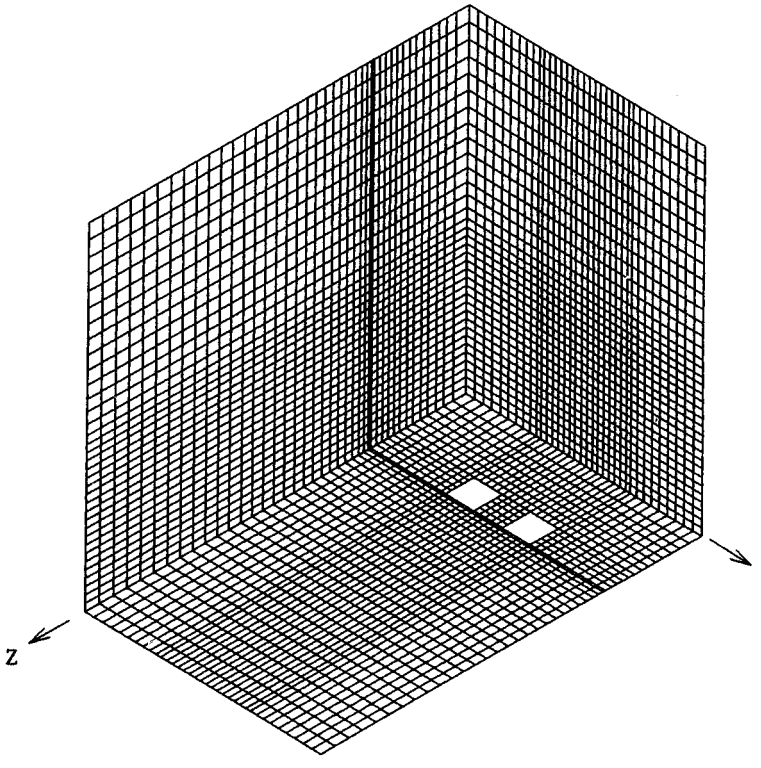

Fig. 2 The grid system ($X \times Y \times Z = 35 \times 35 \times 41$)

the viscous sublayer.

The code was executed on a DEC-α 200 4/100 work station. The iteration was terminated when all the residuals were less than 0.0001. For a typical solution, 3000 to 4000 iterations were required to satisfy the convergence criterion, and the CPU time for a solution was about 1.2 hours.

3. Results and discussions

3.1. The pressure coefficient C_p

Pressure coefficients are defined by

$$C_p = \frac{P - P_0}{\frac{1}{2}\rho U^2} \tag{9}$$

where P_0 is the upstream atmospheric pressure and U is the upstream wind velocity. Contour plots of C_p on the surfaces of the object building are discussed in the following two situations.

3.1.1. Single building

For a 5w-high building, we find that the pressure coefficients have same distributions and values on the surfaces of the building at different wind velocity, as shown in Fig. 3. Thus we conclude that the changes of the wind velocity would not affect the pressure coefficient distribution of the same physical model. The pressure coefficients on the front, top, and back surfaces of the building are symmetry about the center plane and have the same distribution on the two side surfaces. The values of C_p on the front surface are positive and are distributed densely near the top edge and two laterals. The largest pressure coefficient appears in the central area of the front surface.

Due to the tremendous increment of wind velocity, there are very large variations of suction force (the negative pressure coefficient) at the front edge of the roof and the side edges of the two side surfaces. After the wind pass through the roof and front surface, the free space is suddenly open and the fluid flowing downward yields a vortex area around the back of building. This results in the negative C_p corresponding to a suction force on the back surface. The suction force decreases along the downward direction of the back surface. Near the bottom of the building, because of the viscous effect and the no slip condition on the ground surface, another vortex area appears. Thus, the distributions of C_p contour lines concentrate near the top edge and the bottom edge of the back surface of the building.

3.1.2. Twin buildings

The pressure coefficient distributions affected by interfering building B1 on each surface of object building B2 were studied here with a wind velocity of U=15 m/s, 5w high B2 building, three different heights of B1 (i.e., 5w, 10w/3, 5w/2), and three different gaps w/2, w, 3w/2.

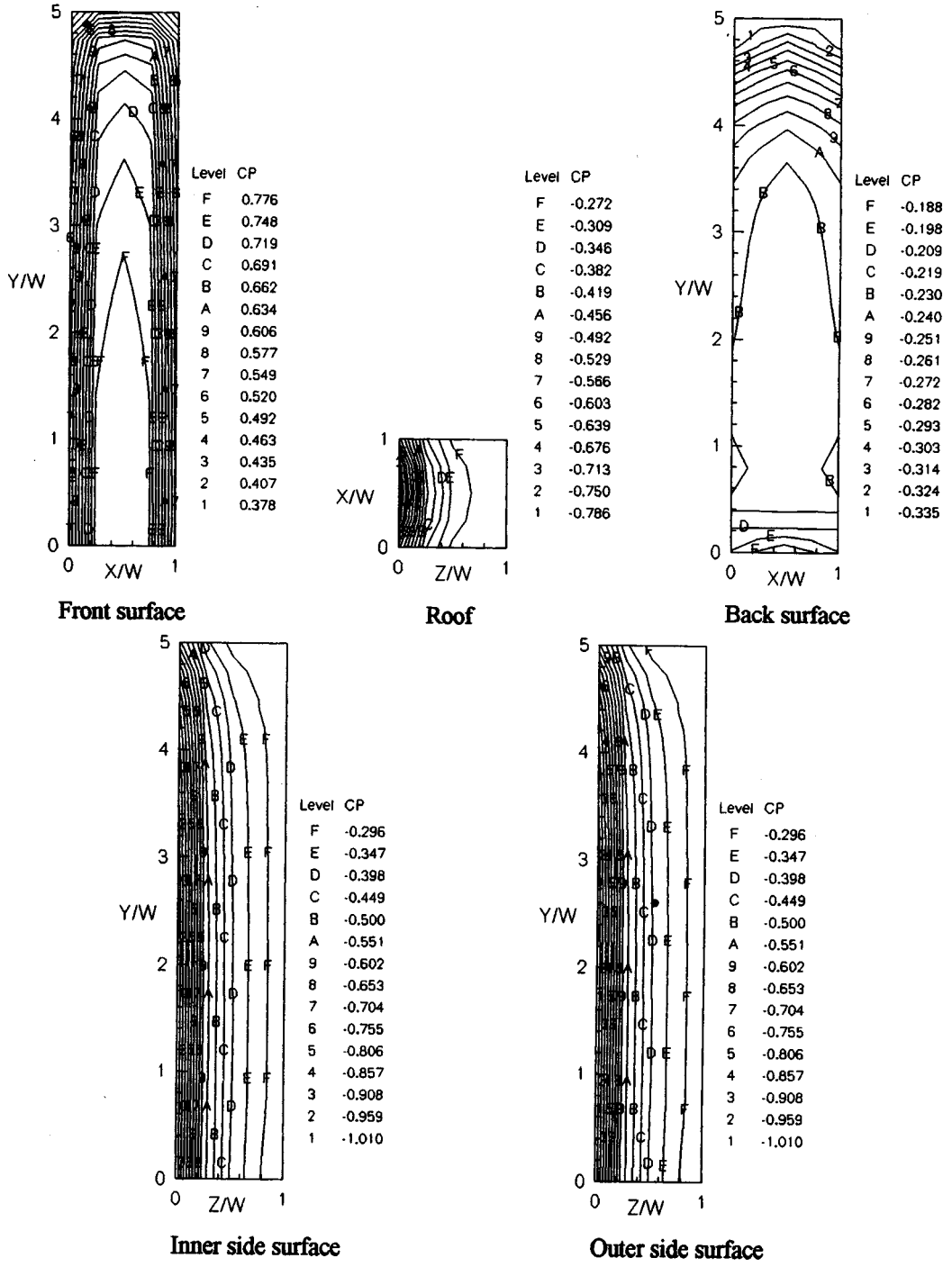

Fig. 3 The distribution of C_p on a 5W (150 m) height single building

Table 2 shows the cases studied in this paper. Figs. 4 to 8 are the distributions of pressure coefficients on each surface of the object building for the interfering cases. The results show

that the pressure coefficient distribution is no longer symmetry about the center plane of the object building because of the mutual interference of two buildings. When the gap is larger and the height of B1 is lower, the interference effect is small and the distribution of C_p approaches to symmetry.

(a) The front surface (-Z) – The figures show that the values of C_p on the front surface are positive, the distributions of C_p are not same as single buildings that have a same symmetrie distribution and the values are much larger. The contour lines of C_p are more sparsely distributed on the interfering side. The largest pressure on the lower central part of the B1 becomes smaller. The smaller gap and the larger height of interfering building cause a larger interference. Thus, the distributions of C_p become more severe unsymmetry and the C_p has a larger value and range than that of a single building.

(b) The inner side surface (-X) – The wind flow between the two buildings is contracted

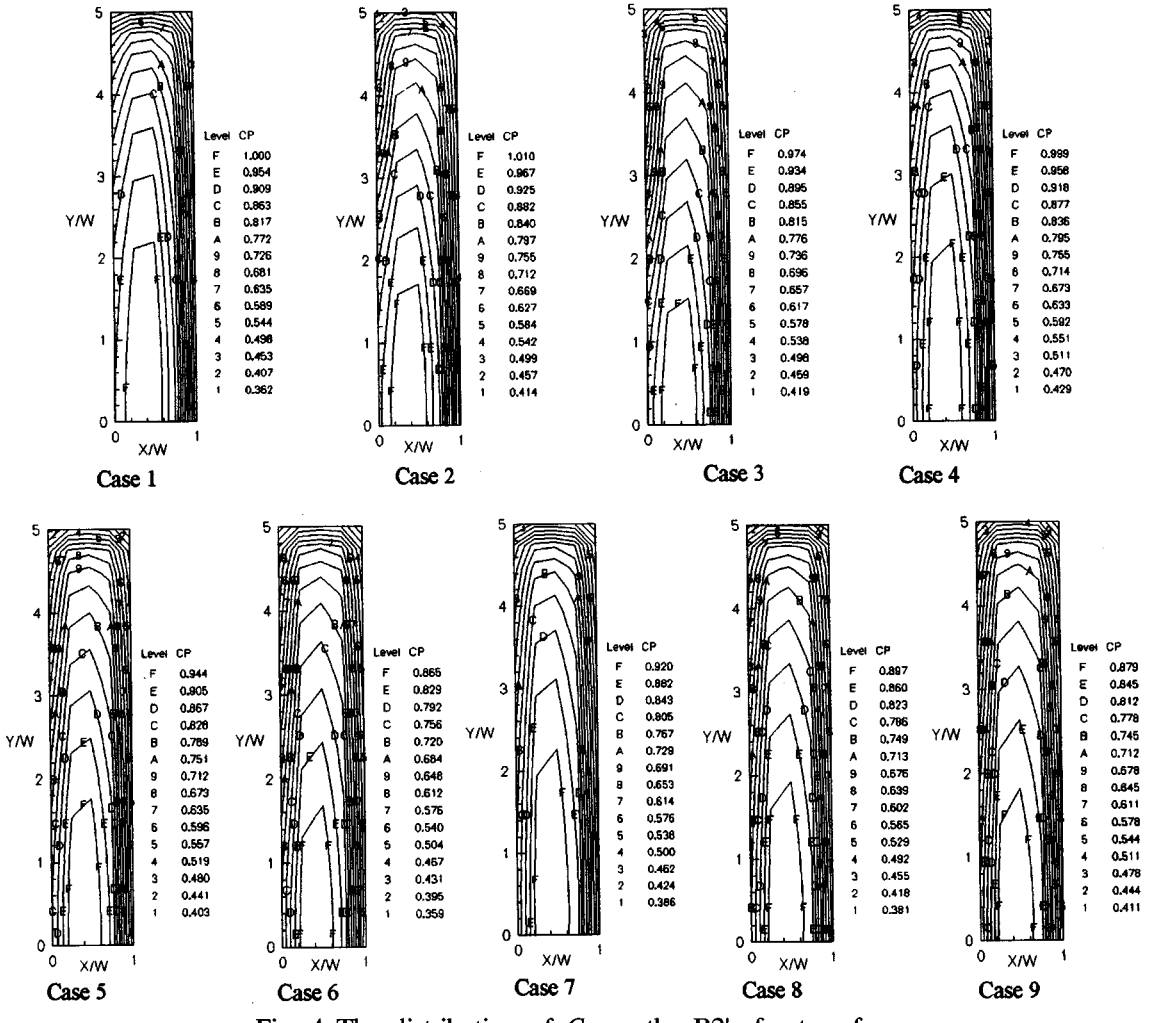

Fig. 4 The distribution of C_p on the B2's front surface

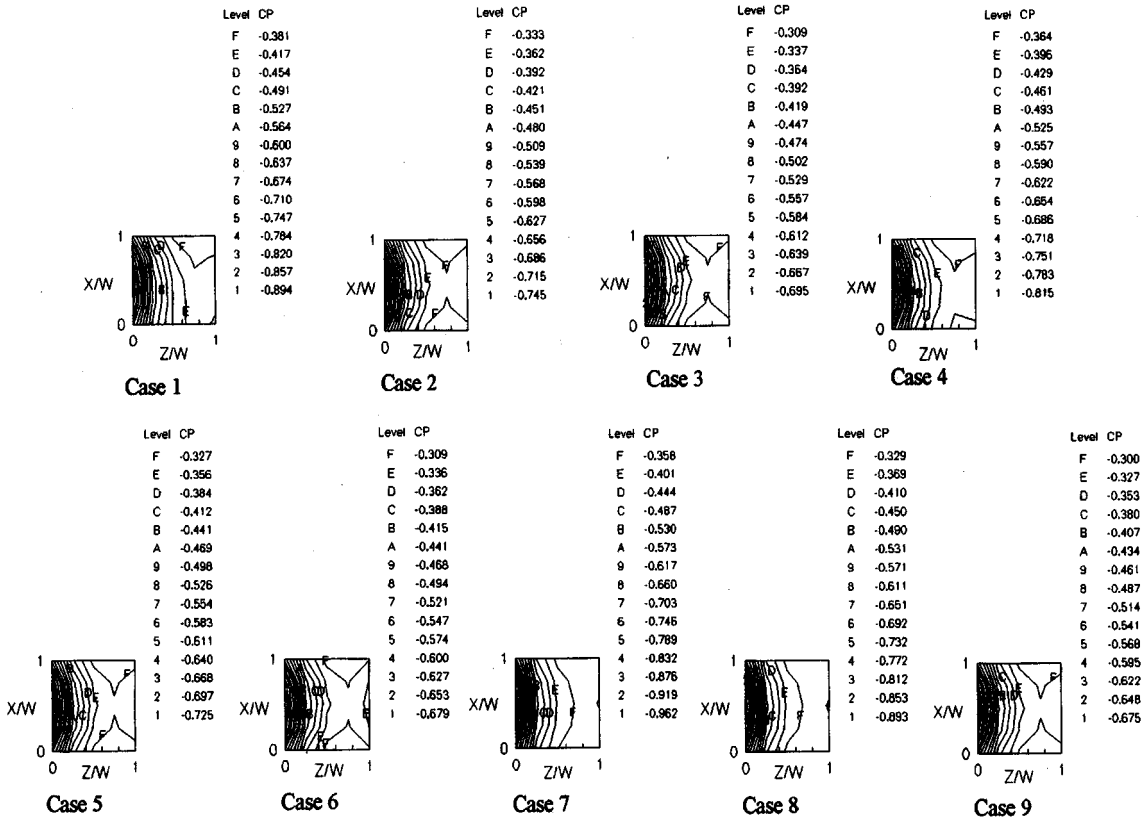

Fig. 5 The distribution of C_p on the B2's roof

and accelerated, and a larger negative value of C_p is generated on the inner side surfaces of two buildings which face each other. This indicates that the twin buildings have stronger suction forces on the inner side surfaces than a single building. As the gap between two buildings increases and/or the height of B1 decrease, the contracting effect decreases and the distribution of pressure coefficient becomes similar to the case of single building. When the height of B1 becomes lower, the pressure coefficient distribution in the region above the height of B1 has a larger variety on the front edge. This is because the fluid of this part has not been blocked by the interfering building B2 and can easily flow through the region. At the blocked region, the amount of the fluid is restrained that makes the fluid velocity more evenly distributed and the pressure coefficient distribution more even as well. The range of C_p is smaller than that of a single building, and increases as the gap and/or the height of B2 decrease.

(c) The outer side surface (+*X*) – The distributions of C_p on the outer side surface of building B2 are similar to those of the single building, but the absolute values and the ranges of C_p are greater than those of the single building bacause of the velocity increment caused by the interference effect. The range of C_p decreases as the gap and/or the height of B1 decrease.

(d) The roof (+*Y*) – The fluid velocity increases a lot at front edge of the top surface that result in a large suction force variation. When two buildings are at the same heights, the

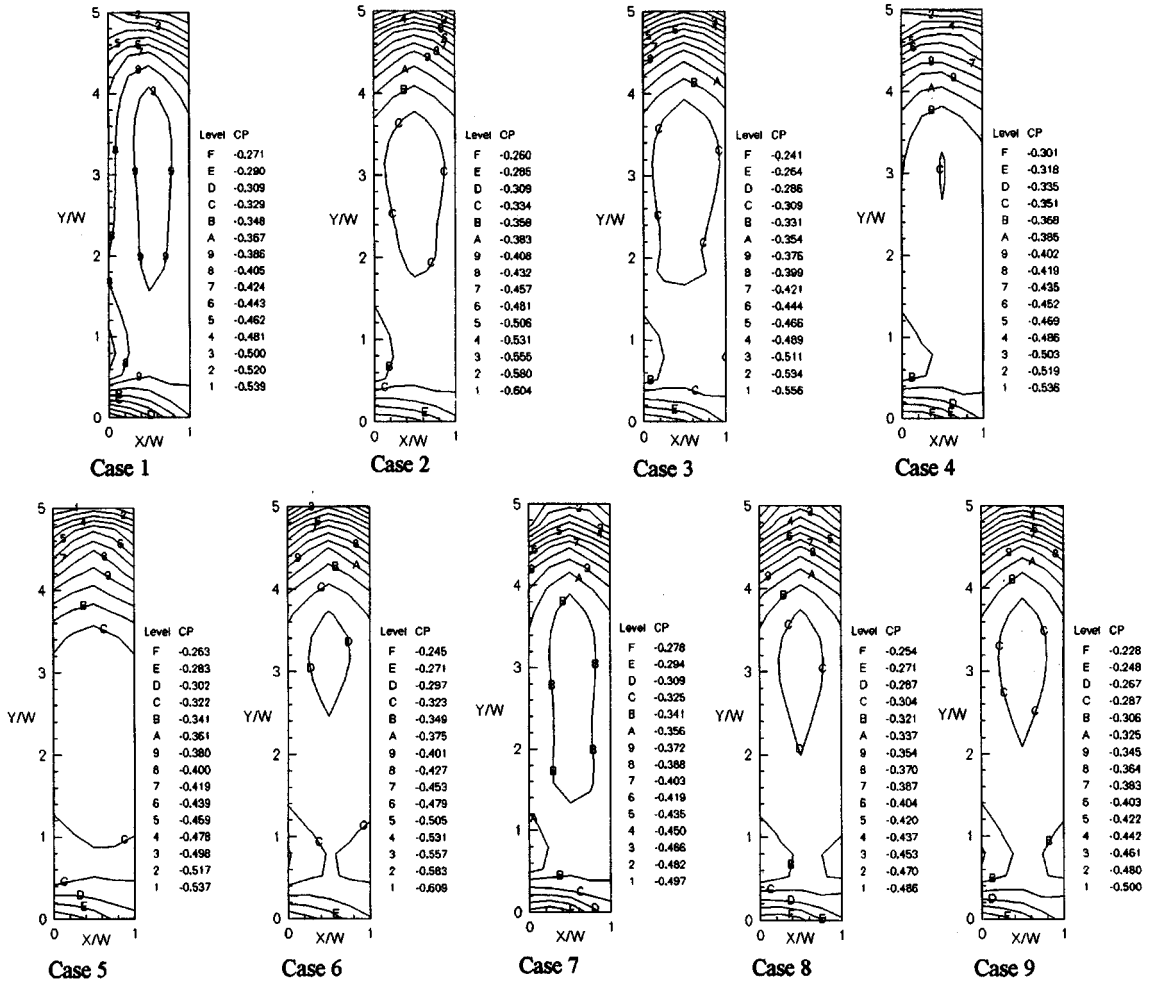

Fig. 6 The distribution of C_p on the B2's back surface

distribution of C_p is not symmetry and is sparse on the interfering side. When B1 is lower than B2, the wind can pass through the region above the B2 more smoothly. Thus, the distribution of C_p becomes closer to a symmetry on the roof as the relative height difference increases. The values and the ranges of C_p becomes smaller as the height of B2 decreases.

(e) The back surface (+Z) – The interfering building causes the increase of vortex strength near the ground surface that also causes the variation of C_p near the bottom. The absolute pressure coefficient values and the ranges of C_p on the back surface were larger when compared with those of a single building. The range of C_p decreases as the gap and/or the height of B1 increases.

3.2. The velocity vector plots

Only the velocity vector plots of a wind speed of 15 m/s are discussed here since they are similar to those of 10, 15 and 20 m/s wind speed. Fig. 9 shows the velocity vector plots

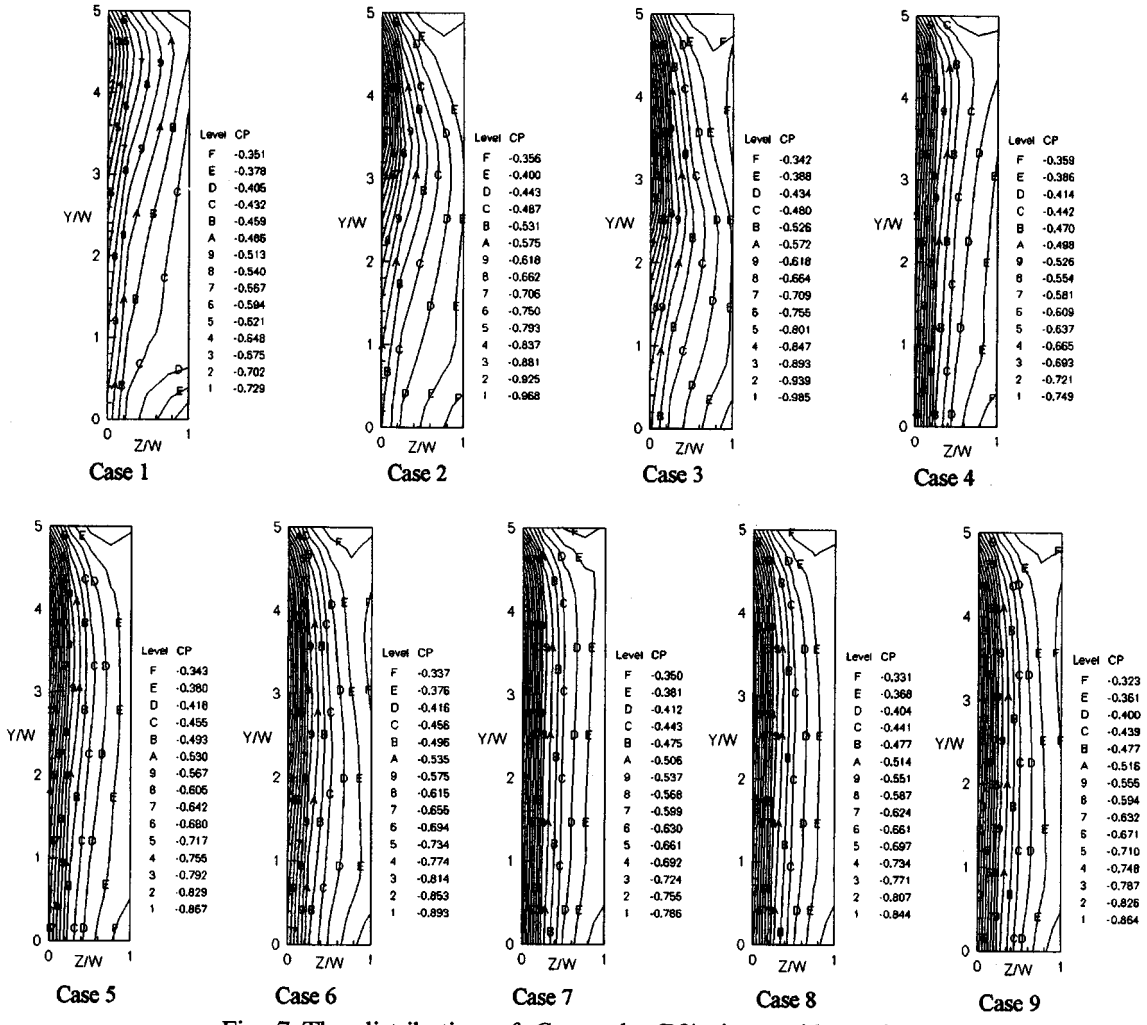

Fig. 7 The distribution of C_p on the B2's inner side surface

around the inner side surface of the object building. A recirculation zone is created at the rear bottom. The stagnation point on the surface of the inner side surface along the ground is far away form the rear bottom for a larger gap and taller interfering building. Fig. 10 shows the velocity vector plots around the buildings at $H_2/2$ height. Two recirculation zones are created behind each building and the flow in the gap inclined to the side of the lower building. When the two buildings have same heights, the velocities along the center line at $H_2/2$ height of two buildings are large for a larger gap but the recirculation zones remain in the similar pattern.

3.3. The velocity on the vertical centerline between two buildings

From Fig. 11, we can see that the velocity curves have a close relationship with the height of interfering building and the gap between two buildings. The velocities on the center line between two buildings and below the height of the interference building are equal to 1.4 to 1.5 times the upstream wind velocity. The velocities is being changed slowly from the bottom to

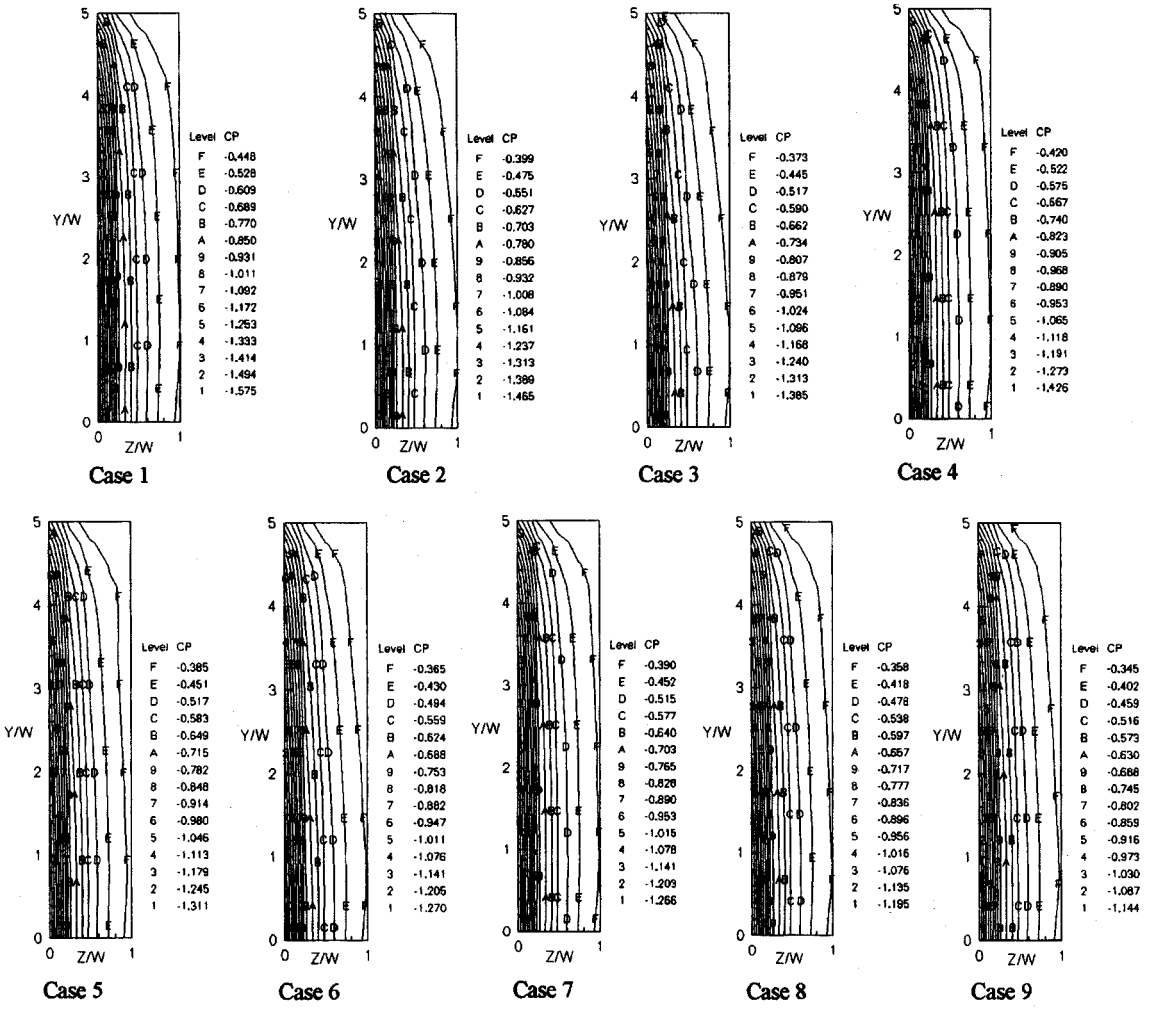

Fig. 8 The distribution of C_p on the B2's outer side surface

Table 2 Cases studied

Case No.	1	2	3	4	5	6	7	8	9
Bl's Height	5 W	10 W/3	5 W/2	5 W	10 W/3	5 W/2	5 W	10 W/3	5 W/2
Gap	W/2	W/2	W/2	W	W	W	3 W/2	3 W/2	3 W/2

the top of the interfering building, then decrease quickly and approach to the free wind velocity at 1.5 time's the height of the object building. When the gap is small, the velocities have sudden changes at the top of interfering building and at that of the object building. When the gap is large, the velocity curves change more smoothly. The velocity is larger for the smaller gap and/or the taller interfering building.

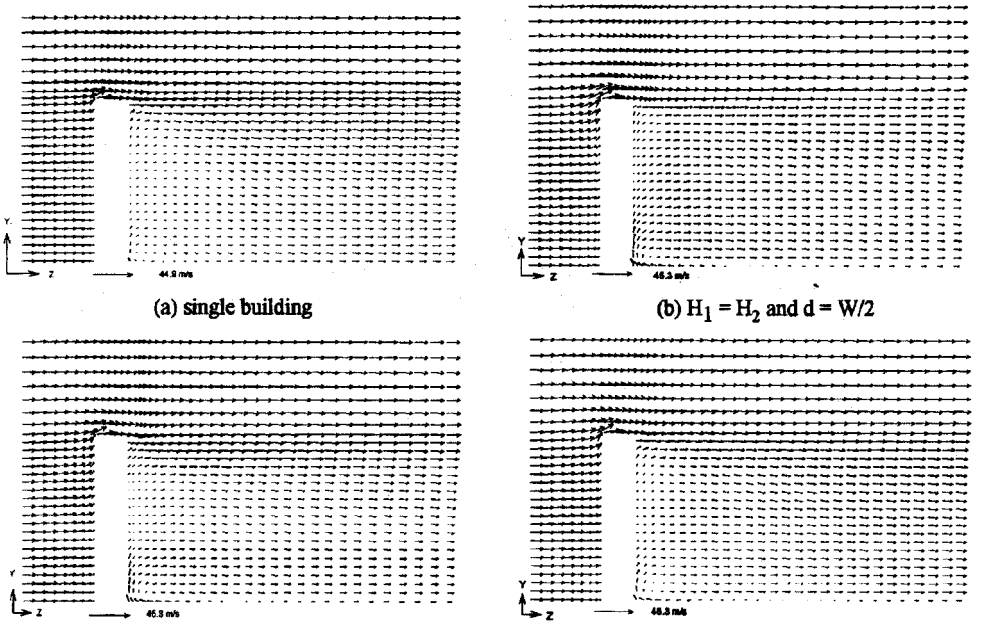

(a) single building

(b) $H_1 = H_2$ and d = W/2

(c) $H_1 = 2\,H_2/3$ and d = W/2

(d) $H_1 = H_2$ and d = W

Fig. 9 The velocity vector around the inner side surface of the object building

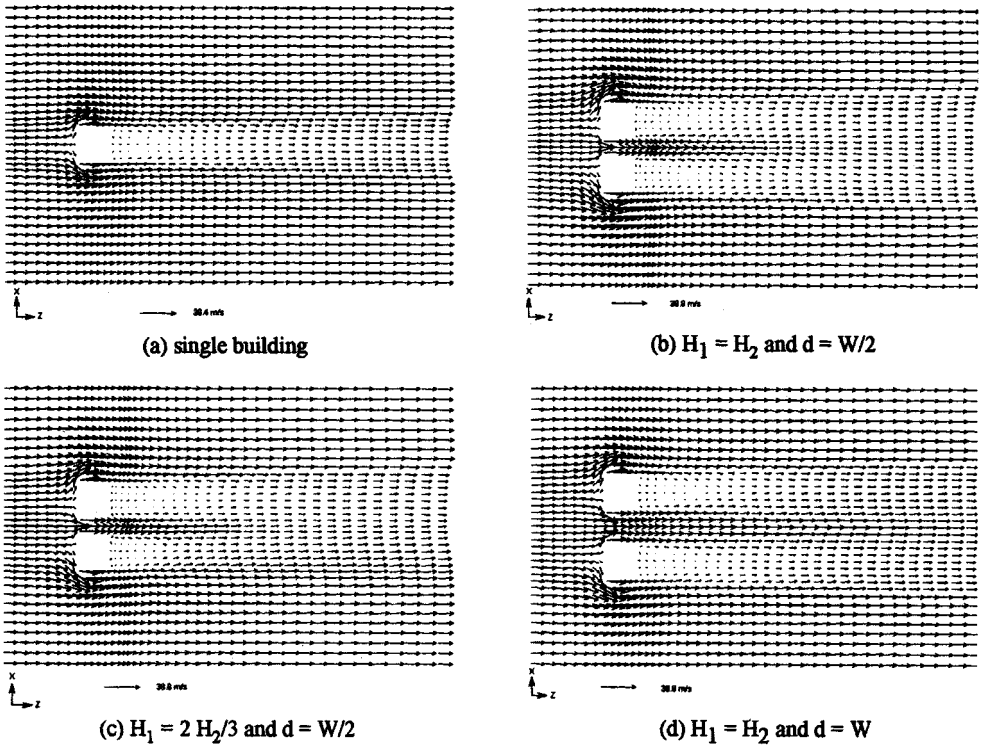

(a) single building

(b) $H_1 = H_2$ and d = W/2

(c) $H_1 = 2\,H_2/3$ and d = W/2

(d) $H_1 = H_2$ and d = W

Fig. 10 The velocity vector around the object building at $Z=H_2/2$

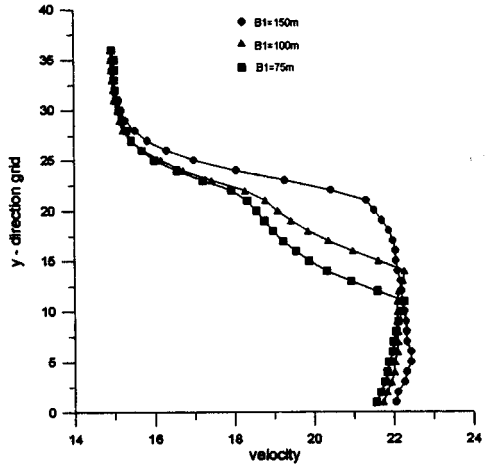

(a) gap = W/2

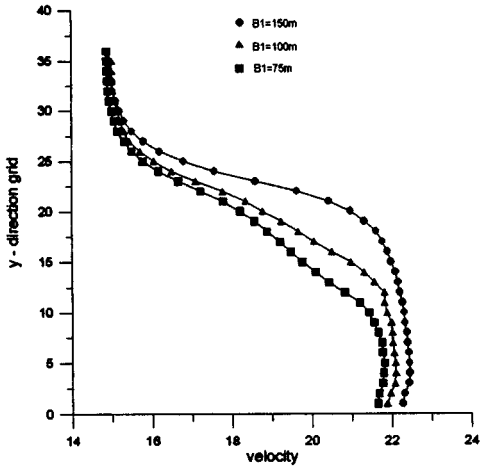

(b) gap = W

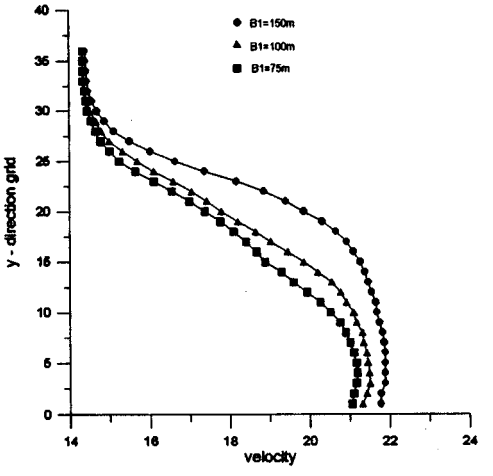

(c) gap = 3W/2

Fig. 11 The velocity on the vertical center line between two buildings

4. Conclusions

The interference effect on a tall square building resulting from the neighboring building of different heights and gaps was investigated. The wind flow between the two buildings was contracted and accelerated, and a stronger suction force was generated on the inner side surfaces. The range of C_p on the inner side surfaces of twin buildings is smaller than that of a single building. When the gap is somewhere between w/2 to 3w/2, the maximum velocity on the center line is 1.4 to 1.5 times the upstream velocity. The pressure coefficient distributions were not symmetry unlike the case of a single building due to the mutual interference of two buildings. The distributions of C_p were more sparse on the interfering side of each surface. This kind of phenomenon is reduced as the gap is increased and/or the height of interfering

building is decreased. Since the neighboring buildings may exhibit significant interaction effects on the object building, the interfering building of different sizes at various locations need to be dealt with in the future study.

References

Launder B.E. and Spalding D.B. (1974), "The numerical computation of turbulent flows", *Computer Methods in.Applied Mechanics and Engineering*, **3**, 269-289.

Murakami S. and Mochida A. (1989), "Three-dimensional numerical simulation of turbulent flow around buildings using the k-ε-turbulence model", *Building and Environment*, **24**(1), 51-64.

Patankar S.V. (1981), "A calculation procedure for two-dimensional elliptic problem", *Numerical Heat Transfer*, **4**, 409-426.

Paterson D.A. and Apelt C.J. (1989), "Simulation of wind flow around three-dimensional buildings", *Building and Environment*, **24**(1), 39-50.

Qasim A., Maxwell T.T. and Parameswaran S. (1992), "Computation predictions of flow over a 2-D building", *Journal of Wind Engineering and Industrial Aerodynamics*, **41-44**, 2839-2840.

Stathopoulos T. and Zhou Y.S. (1993), "Computation of wind pressure on L-shaped building", *Journal of Engineering Mechanics, ASCE*, **119**(8), 419-430.

Taniike Y. (1992), "Interference mechanism for enhanced wind forces on neighboring tall buildings", *Journal of Wind Engineering and Industrial Aerodynamics*, **41-44**, 1073-1083.

(Communicated by Chang-Koon Choi)